Chapter 5
Performance Evaluation of Grid-Connected Solar Photovoltaic (SPV) System with Different MPPT Controllers

R. Singh and B. S. Rajpurohit

Abstract Renewable energy plays an important role in electric power generation. Solar energy is one of them. It has the advantage of no pollution, low maintenance cost, no installation area limitation, and no noise due to the absence of the moving parts. However, high initial cost and low conversion efficiency have deterred its popularity. Due to the non-linear relation between the voltage and current of the PV cell, it is observed that there is unique Maximum Power Point (MPP) at particular environmental conditions, and this peak power point keeps changing with solar irradiations and ambient temperature. To achieve high efficiency in SPV power generation it is required to match the SPV source and load impedance properly for any weather conditions, thus obtaining maximum power generation. The technique process of MPP is being tracking which is called Maximum Power Point Tracking (MPPT). In recent years, a large number of techniques have been proposed for MPPT and some based on Computational Intelligence (CI) techniques. In this chapter performance evaluation of DC–DC boost converter based on P&O and INC has been compared. The scope of the work is to first give the detailed mathematical model of grid connected three-phase SPV system. A parametric model of SPV cell is presented. Second, thermal modeling and switching loss calculation of switching devices has been discussed and then the performance evaluation will be carried out for P&O and INC based MPPT algorithms for various operating conditions of the SPV array, in terms of energy injected to grid, switching losses, junction temperature and sink temperature, for switching in the DC–DC boost converter. Application of an Adaptive Neuro-Fuzzy Inference Systems (ANFIS) based intelligent controller has been described and

R. Singh (✉) · B. S. Rajpurohit
School of Computing and Electrical Engineering, Indian Institute of Technology,
Mandi, Himachal Pradesh, India
e-mail: er.ranjitsingh2010@gmail.com

B. S. Rajpurohit
e-mail: bsr@iitmandi.ac.in

applied for fast, accurate, and efficient control of DC–DC boost converter used for SPV system, in place of conventional (PI) controllers.

5.1 Introduction

In the current century, the world is increasingly experiencing a great need for additional energy resources so as to reduce the dependency on conventional sources, and photovoltaic energy could be an answer to that need. Generally a Solar Photovoltaic (SPV) system can be divided into three categories: stand alone, grid-connection and hybrid system. For places that are far away from a conventional power generation system, standalone power generation systems have been considered a good alternative. These systems can be seen as a well-established and reliable economic source of electricity in rural areas, especially where the grid power supply is not fully extended. Solar energy has the advantage of no pollution, low maintenance cost, no installation area limitation, and no noise due to the absence of the moving parts. However, high initial cost and low conversion efficiency have deterred its popularity. Therefore, it is important to reduce the installation cost and to increase the energy conversion efficiency of SPV arrays and the power conversion efficiency of SPV system. Due to the non-linear relation between the voltage and current of the PV cell, it is observed that there is unique Maximum Power Point (MPP) at particular environmental conditions, and this peak power point keeps changing with solar irradiations and ambient temperature. To achieve high efficiency in SPV power generation it is required to match the SPV source and load impedance properly for any weather conditions, thus obtaining maximum power generation. Hence, tracking the MPP of a SPV array is usually an essential part of a SPV system. Maximum power extraction can be obtained by a method called as Maximum Power Point Tracking (MPPT). As such, many MPPT methods have been developed and implemented. The methods vary in complexity, sensors required, convergence speed, cost, range of effectiveness, implementation hardware, popularity, and in other respects. They range from the almost obvious (but not necessarily ineffective) to the most creative (not necessarily most effective). In fact, so many methods have been developed that it has become difficult to adequately determine which method, newly proposed or existing, is most appropriate for a given PV system. Given the large number of methods for MPPT, a survey of the methods would be very beneficial to researchers and practitioners in PV systems [1]. In recent years, a large number of techniques have been proposed for MPPT such as Constant Voltage Tracking (CVT), the Perturb-and-Observe (P&O) method, the Incremental Conductance

(INC) method, and some based on Computational Intelligence (CI) techniques. Computational intelligence (CI) techniques, such as fuzzy logic (FL), artificial neural network (ANN), and evolutionary computation (EC), are recently promoted for the control of systems. Overall, the dynamic performance of a system can be substantially improved by the introduction of CI based techniques for the intelligent control. The broad categories for different MPPT are given bellow:

Conventional Algorithms

- Curve Fitting Method
- Perturb and Observe
- Incremental Conductance
- Fractional Open-Circuit Voltage
- Fractional Short-Circuit Current
- Ripple Correlation Control (RCC)
- Current Sweep
- DC Link Capacitor Droop Control.

Computational Intelligence Based Techniques

- Fuzzy Logic Control (FLC)
- Artificial Neural Network (ANN)
- Genetic Algorithm (GA)
- Hybrid methods (such as ANFIS).

This chapter presents a performance analysis of grid connected SPV system for different MPPT algorithms. The performance evaluation of DC–DC boost converter based on P&O and INC has been compared in this chapter. The scope of the work is to first give the detailed mathematical model of grid connected three-phase SPV system. A parametric model of SPV cell is presented. Second, thermal modeling and switching loss calculation of switching devices has been discussed and then the performance evaluation will be carried out for different MPPT algorithms for various operating conditions of the SPV array, in terms of energy injected to grid, switching losses, junction temperature and sink temperature, for switching in the DC–DC boost converter. In this work, a computational strategy directed more towards intelligent behavior is employed as a tool for controlling DC–DC converter employed in SPV system. The conventional proportional-integral (PI) controller is replaced with a nonlinear adaptive neuro-fuzzy inference system (ANFIS) based controller, that is applied for fast, accurate, and efficient control of DC–DC boost converter used for SPV system. The design and procedure for selection of parameters and training of ANFIS are described. The performance of the conventional PI and ANFIS based controllers is compared using simulation results on a test system.
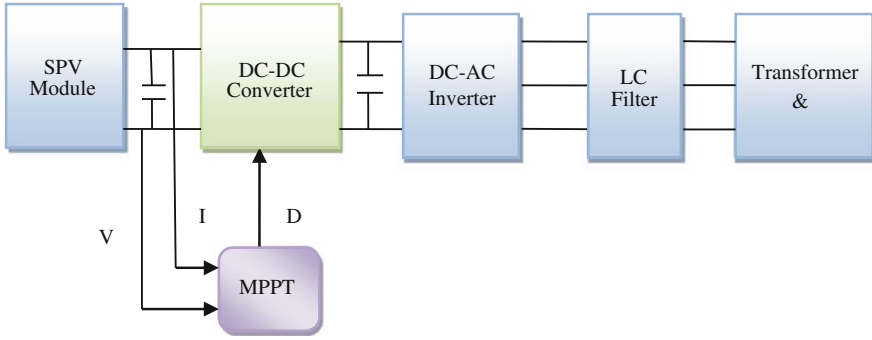
Fig. 5.1 Schematic diagram of SPV system blocks

5.2 Three-Phase Solar Photovoltaic System

The configuration of the solar power generation system is as shown in Fig. 5.1. In this system sunlight is captured by SPV array. The SPV array is connected a DC–DC converter to increase the voltage level and to operate at the desired current and desired voltage to match the maximum available power from the PV module. This MPPT DC–DC converter is followed by a DC–AC inverter for grid connection or to supply power to the AC loads in stand-alone applications. The grid connected SPV array system is thus composed of the following blocks:

- Solar Photovoltaic Array
- DC–DC Boost Converter and Controller
- DC Link Capacitor
- DC–AC Three Phase Inverter and Controller
- LC Filter
- Transformer
- Grid.

5.3 Solar PV Cell

The equivalent circuit of the solar PV cell is given below in Fig. 5.2. I_{ph} is the cell photocurrent that is proportional to solar irradiation, I_{rs} is the cell reverse saturation current that mainly depends upon the temperature, K_o is a constant, N_s and N_p are the number of series and parallel strings in the PV array respectively, R_{sh} and R_p is the series and parallel resistance of the PV array. Generally, a PV module comprises of a number of PV cells connected in either series or parallel and its mathematical model can be simply expressed as given below. The equation describing the I–V characteristics of the solar array are as follows [2]:
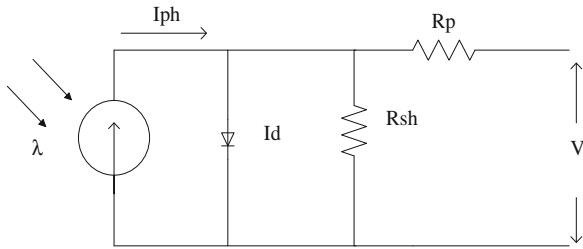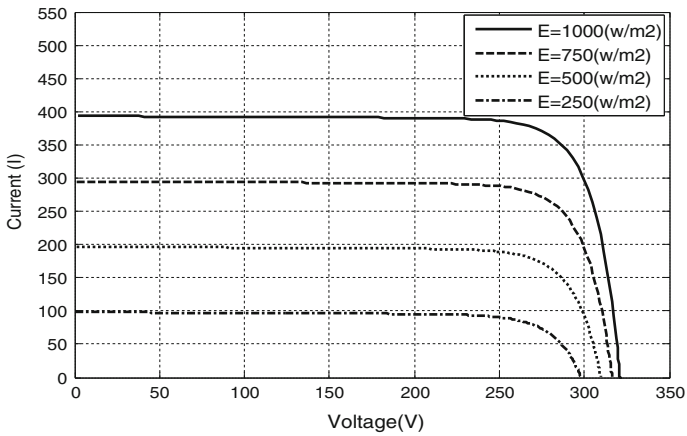
Fig. 5.2 Equivalent circuit of solar cell

Fig. 5.3 Simulated *I–V* curve of a SPV module for varying irradiance condition at 25 °C temperature
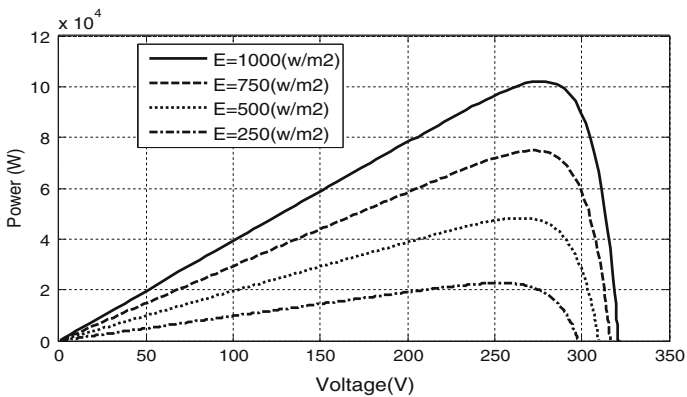

Fig. 5.4 Simulated *P–V* curve of a SPV module for varying irradiance condition at 25 °C temperature

Table 5.1 Specification from sun power module (SPR-305) data sheet	No of series connected cells	96
	Open circuit voltage (V_{oc})	64.2 V
	Short circuit current (I_{sc})	5.96 A
	Maximum power	100.7 kW
	Voltage at maximum power (V_{mpp})	54.7 V
	Current at maximum power (I_{mpp})	5.58 A

Fig. 5.5 Schematic of a DC–DC boost converter
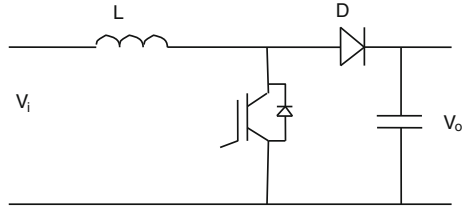
$$I = N_p I_{ph} - N_p I_{rs} \left[\exp\left(K_o \frac{V}{N_s} \right) - 1 \right] \tag{5.1}$$

where, I denotes the PV array output current, V is the PV array output voltage. All of the constants in the above equation can be determined by examining the manufacturer rating of the SPV array and then the published or measured I–V curves of the array as described in Table 5.1. Simulated *I–V* and *P-V* curve of a SPV module for varying irradiance condition at 25 °C temperature are shown in Figs. 5.3 and 5.4, respectively. As a typical case, the Sun Power modules (SPR-305) array is used to illustrate and verify the model. The model parameters are given in Table 5.1 and can be found in the datasheet [3].

5.4 Voltage Boost DC–DC Converter and MPPT Algorithms

For maximum energy exploitation it is reasonable to operate SPV at the MPP. The SPV array is connected a DC–DC boost converter to increase the voltage level and to operate at the desired current and desired voltage to match the maximum available power from the PV module. The simplest form of DC–DC boost converter based on single switch and input inductor is used. The boost topology is capable of raising input voltage to the intermediate DC-link voltage, with the only limitation due to efficiency drop at very low voltage [4]. The DC–DC boost converter equivalent circuit is shown in Fig. 5.5, depending on the load and the circuit parameters, the inductor current can be either continuous or discontinuous. The inductor value, L, required to operate the converter in continuous conduction mode is calculated such that the peak inductor current at maximum output power does not exceed the power switch current rating. Thus, L and output capacitor value, C, to give the desired peak-to-peak output ripple is calculated as:

$$L = \frac{(1-D)^2}{2f} \tag{5.2}$$

$$C \geq \frac{DV_0}{V_r R f} \tag{5.3}$$

where f is switching frequency, D is duty cycle of the IGBT switch, R is the load resistance, V_o is output voltage and V_r is peak-to-peak ripple voltage. The DC–DC boost converter has the following simplified input-output equation.

$$V_i = (1-D)V_o \tag{5.4}$$

where V_o is the DC-link voltage regulated to be constant by the DC-link PI controller based voltage control. So D is the degree of freedom to change the work point of the SPV cells.

The Fig. 5.4 shows the char *P–V* characteristics of solar cells. The problem considered by MPPT techniques is to automatically find the voltage and current of at which a SPV array should operate to obtain the maximum power output under a given temperature and irradiance. It is noted that under partial shading conditions, in some cases it is possible to have multiple local maxima, but overall there is still only one true MPP. Most techniques respond to changes in both irradiance and temperature, but some are specifically more useful if temperature is approximately constant. Most techniques would automatically respond to changes in the array due to aging, though some are open-loop and would require periodic fine-tuning [1]. Systems composed of various PV modules located at different positions should have individual power conditioning units to ensure the MPPT for each module. The various MPPT algorithms are briefly described as given below.

5.4.1 Fractional Open-Circuit Voltage Based MPPT

The near linear relationship between voltage at maximum power (V_{MPP}) and Open Circuit Voltage (V_{OC}) of the PV array, under varying irradiance and temperature levels, has given rise to the fractional V_{OC} method [5–12].

$$V_{MPP} \approx k_1 V_{OC} \tag{5.5}$$

where k_1 is a constant of proportionality. Since k_1 is dependent on the characteristics of the PV array being used, it usually has to be computed beforehand by empirically determining V_{MPP} and V_{OC} for the specific PV array at different irradiance and temperature levels. The factor k_1 has been reported to be between 0.71 and 0.78. Once k_1 is known, V_{MPP} can be computed using (5.5) with V_{OC} measured periodically by momentarily shutting down the power converter. Figure 5.6 shows the implementation of fractional open-circuit based MPPT.
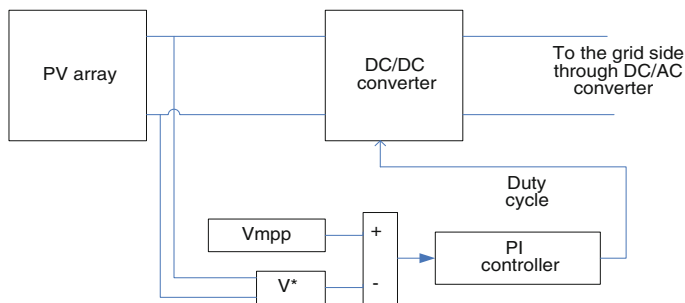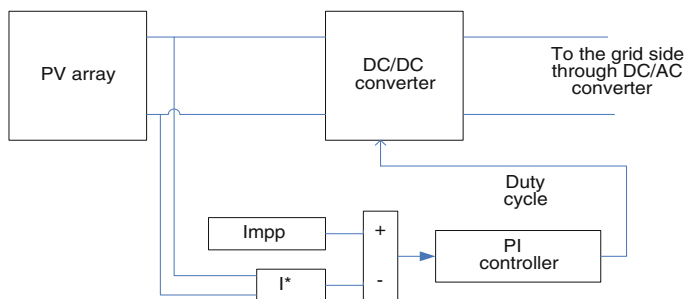
Fig. 5.6 Fractional open-circuit based MPPT

Fig. 5.7 Fractional short-circuit based MPPT

5.4.2 Fractional Short-Circuit Current Based MPPT

Fractional I_{SC} results from the fact that, under varying atmospheric conditions, I_{MPP} is approximately linearly related to the I_{SC} of the PV array [13–15].

$$I_{MPP} \approx k_2 I_{SC} \tag{5.6}$$

where k_2 is a proportionality constant. Just like in the fractional V_{OC} technique, k_2 has to be determined according to the PV array in use. The constant k_2 is generally found to be between 0.78 and 0.92. Figure 5.7 shows the implementation of fractional short-circuit based MPPT.

5.4.3 Perturb and Observe Based MPPT

Perturb and Observe (P&O) involves a perturbation in the duty ratio of the power converter, i.e. a perturbation in the operating voltage of the PV array. In the case of a PV array connected to a power converter, perturbing the duty ratio of power converter perturbs the PV array current and consequently perturbs the PV array voltage [16–25]. From Fig. 5.3, it can be seen that incrementing the voltage
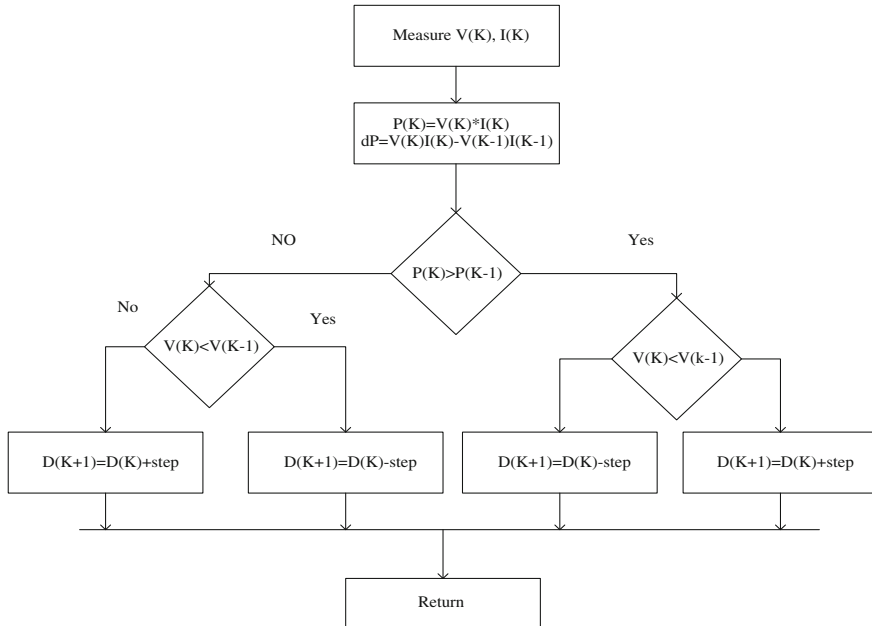
Fig. 5.8 Flow chart of P&O based MPPT

increases the power when operating on the left of the MPP and decreases the
power when on the right of the MPP. Therefore, if there is an increase in power,
the subsequent perturbation should be kept the same to reach the MPP and if there
is a decrease in power, the perturbation should be reversed. The flow chart of the
P&O based method is given in Fig. 5.8.

5.4.4 Incremental Conductance Based MPPT

The incremental conductance is based on the fact that the slope of the PV array
power curve is zero at the MPP, positive on the left of the MPP and negative on the
right [26–35]. The MPP can be thus be tracked by comparing the instantaneous
conductance (I/V) to the incremental conductance ($\Delta I/\Delta V$).

So,

$$\begin{cases} dP/dV = 0 \\ dP/dV > 0 \\ dP/dV < 0 \end{cases}. \tag{5.7}$$

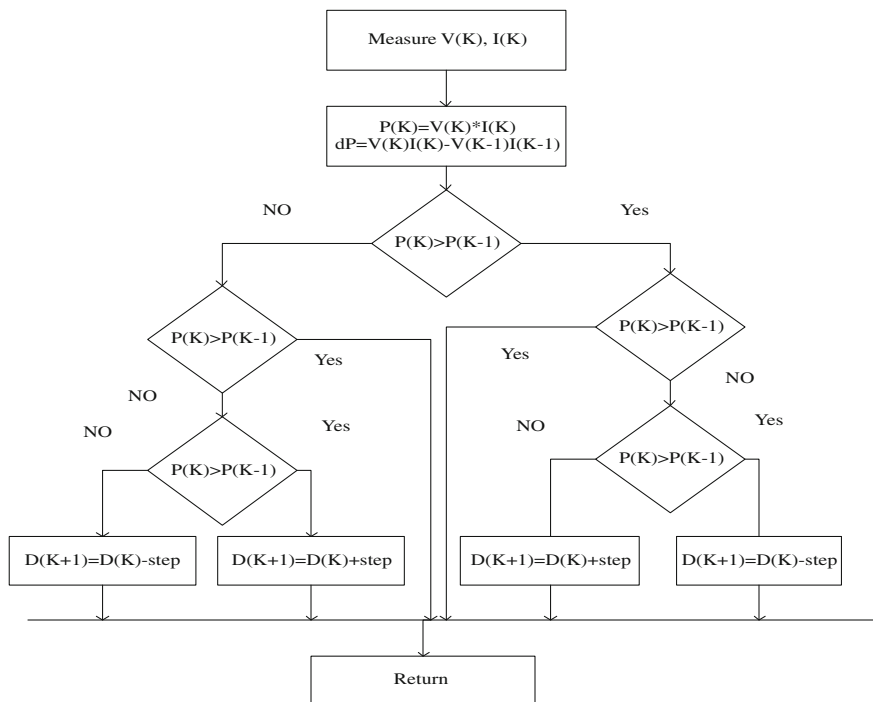The flow chart of the INC algorithm is given in Fig. 5.9.

Fig. 5.9 Flow chart of INC based MPPT

5.4.5 *Fuzzy Logic Control Based MPPT*

Fuzzy logic controllers (FLC) have the advantages of working with imprecise inputs, not needing an accurate mathematical model, and handling nonlinearity. FLC generally consists of three stages: fuzzification, rule base lookup table, and defuzzification. During fuzzification, numerical input variables are converted into linguistic variables based on a membership function. In this case, rule base are given in Table 5.2. The inputs to a MPPT fuzzy logic controller are usually an error E and a change in error ΔE. The user has the flexibility of choosing how to compute E and ΔE. Since dP/dV vanishes at the MPP [36–40]. By calculate the following

$$E(n) = \frac{P(n) - P(n-1)}{V(n) - V(n-1)} \tag{5.8}$$

$$\Delta E(n) = E(n) - E(n-1). \tag{5.9}$$

Then the error signal can be calculated as

Table 5.2 Fuzzy rule base table [40]

ΔE	NB	NS	ZE	PS	PB
E					
NB	ZE	ZE	NB	NB	NB
NS	ZE	ZE	NS	NS	NS
ZE	NS	ZE	ZE	ZE	ZE
PS	PS	PS	PS	ZE	ZE
PB	PB	PB	PB	ZE	ZE

$$E(n) = \frac{I}{V} + \frac{dI}{dV}.$$

Once E and ΔE are calculated and converted to the linguistic variables, the fuzzy logic controller output, which is typically a change in duty ratio ΔD of the power converter, can be looked up in a rule base Table 5.2. Implementation of a fuzzy logic controller based MPPT is shown in Fig. 5.10.

5.4.6 Artificial Neural Network

Another intelligent technique is the artificial neural network. Neural networks commonly have three layers: input, hidden, and output layers. The number of nodes in each layer vary and are user-dependent. The input variables can be PV array parameters like V_{OC} and I_{SC}, atmospheric data like irradiance and temperature, or any combination of these. The output is usually one or several reference signal(s) like a duty cycle signal used to drive the power converter to operate at or close to the MPP [39–42]. The most commonly used neural network in the MPPT is feed forward neural network.

Since most PV arrays have different characteristics, a neural network has to be specifically trained for the PV array with which it will be used. The characteristics of a PV array also change with time, implying that the neural network has to be periodically trained to guarantee accurate MPPT. Implementation of ANN based MPPT is shown in Fig. 5.11.

5.4.7 Genetic Algorithm

A genetic algorithm (GA) is a procedure used to find approximate solutions to search problems through application of the principles of evolutionary biology. The evolutionary process of a GA is a highly simplified and stylized simulation of the biological version. It starts from a population of individuals randomly generated according to some probability distribution, usually uniform and updates this population in steps called generations. Each generation, multiple individuals are randomly selected from the current population based upon some application of
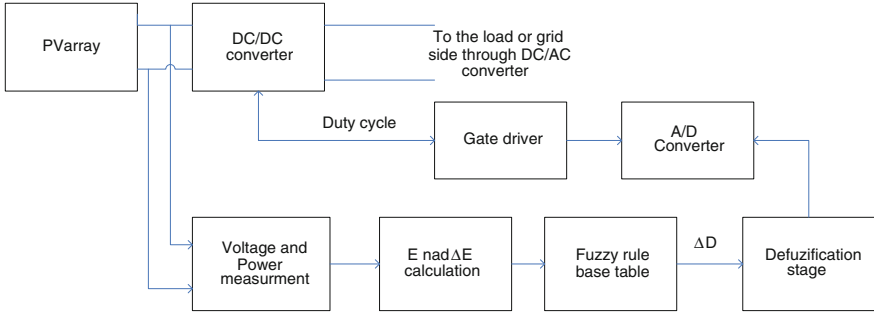
Fig. 5.10 Implementation of a fuzzy logic controller based MPPT
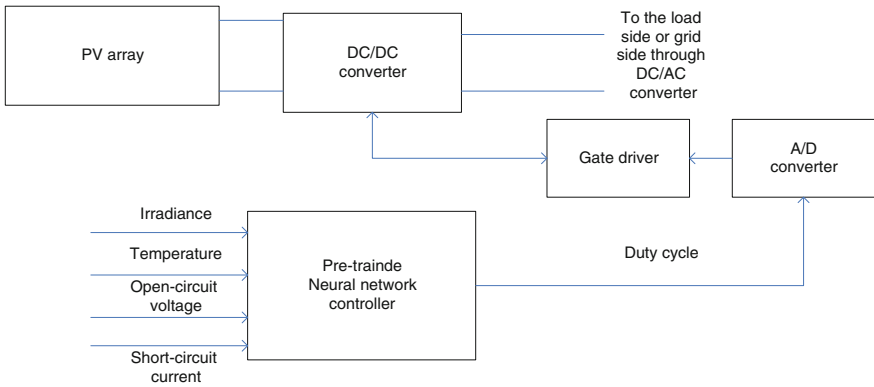
Fig. 5.11 Implementation of ANN based MPPT

fitness, bred using crossover, and modified through mutation to form a new population.

5.5 Three-Phase Inverter for Grid Current SPV System

This MPPT DC–DC converter is followed by a DC–AC inverter for grid connection or to supply power to the AC loads in stand-alone applications. The basic operation principle of the DC–AC inverter is to keep the dc-link voltage at a reference value meanwhile keep the frequency and phase of output current are same as grid voltage. The error signal generated from voltage comparison is adjusted by voltage adjuster and it decides the value of reference current, then it's used to switch ON and OFF the values of the inverter. The load of the grid-connected inverter is power grid, grid power is controlled by grid current [43]. Figure 5.12 shows the schematic of three-phase gird connected inverter. Assume
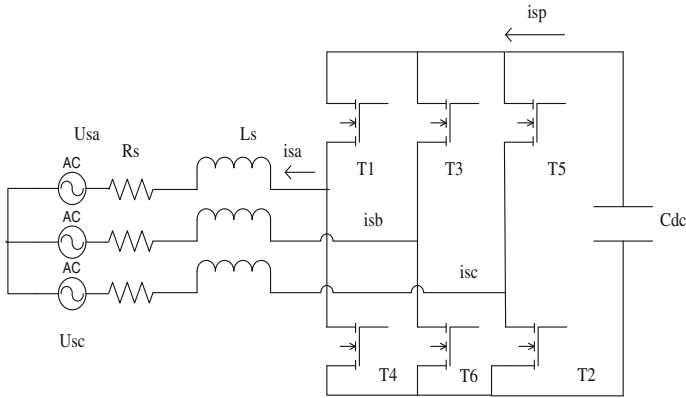
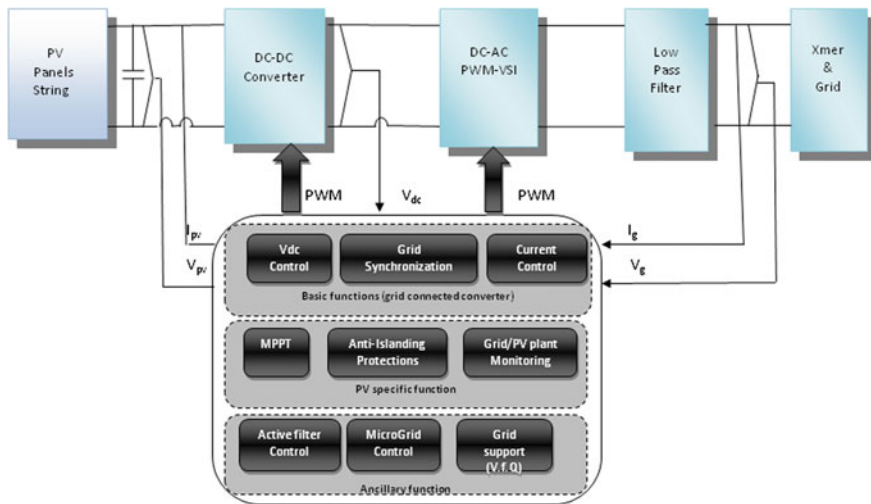**Fig. 5.12** Schematic of three-phase grid connected inverter

Fig. 5.13 Generalized control structure of the SPV system

that three-phase grid voltage is symmetrical, stable and internal resistance is zero; three phase loop resistance R_S and L_S are of the same value respectively; switching loss and on-state voltage is neglectable; affection of distribution parameter is neglectable; switching frequency of the rectifier is high enough.

The generalized control structure of SPV system is shown in Fig. 5.13.

Following are the three different classes of control functions of power electronics converter of SPV system.

1. Basic functions-common for all grid connected inverters

- Grid current control

– THD limits imposed by standards
– Stability in the case of large grid impedance variations
– Ride through grid voltage disturbances
• DC voltage control

– Adaptation to grid voltage variation
– Ride-through grid voltage disturbance
• Grid synchronization

– Operation at the unity power factor as required by standards
– Ride through grid voltage disturbances
2. PV specific functions-common for all PV inverters

• Maximum power point tracking (MPPT)

– Very fast MPPT efficiency during steady state (typically >99 %)
– Stable operation at very low irradiance levels
• Anti-islanding (AI), as required by standards (VDE 0126, IEEE 1574, etc.)
• Grid monitoring

– Synchronization
– Fast voltage/frequency detection for passive AI
• Plant monitoring

– Diagnostic of PV panel array
– Partial shading detection
3. Ancillary functions

• Grid support

– Local voltage control
– Q compensation
– Harmonic compensation
– Fault ride through.

5.6 Power Losses and Junction Temperature Estimation of Semiconductor Devices Used in Power Electronics Convertor of SPV System

As with the increased application and usage of semi-conductor devices the estimation of the power loss and temperature of the junction and thermal model (case and sink) has become a major issue with the increase of the capacity and switching frequency of devices. One method for estimation of power loss of devices is based on the exact current and voltage waveforms of the devices. But, it is very difficult to get the waveforms from simulating each pulse of PWM exactly, with the variation of current and voltage. Usually the power loss is calculated under the

Fig. 5.14 Power loss estimation
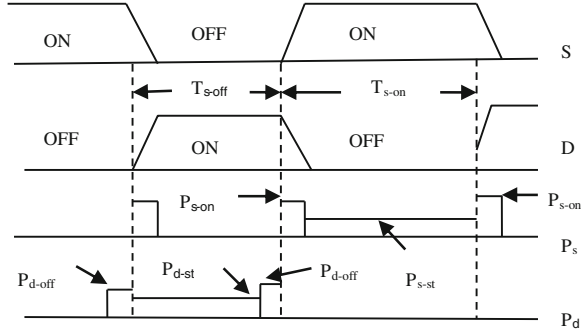
constant junction temperature. However, the power loss does depend on the junction temperature, not only the loss of saturation, but also the loss of transient switching operation. Therefore, the power loss estimation and the junction temperature calculation should be combined to find out the working point of devices [43]. The power loss of each switching operation of semiconductor device (IGBT) is divided into three main portions, which are illustrated in Fig. 5.14. Total power loss during each pulse of the IGBT is the sum of turn-on loss, turn-off loss, and saturation loss. Also, the losses of the anti-paralleled diode are included, if any.

It can be assumed that the IGBT power loss of turn-on or turn-off depends on the dc-link voltage and collector current of the IGBT. From application, it was found that the transient switching waveforms change with increase of junction temperature (50). It should be pointed out that the turn-on loss and turn-off loss are also functions of junction temperature which are expressed in (5.10), (5.11), (5.13), and (5.14). The saturation voltage of the IGBT and its antiparallel diode is usually defined as the function of junction temperature and collector current which are shown in (5.12) and (5.15).

$$P_{s-on} = f_{s-on}(V_d, i, T_j) \tag{5.10}$$

$$P_{s-off} = f_{s-off}(V_d, i, T_j) \tag{5.11}$$

$$V_{s-st} = f_{s-st}(i, T_j) \tag{5.12}$$

$$P_{d-on} = f_{d-on}(V_d, i, T_j) \tag{5.13}$$

$$P_{d-off} = f_{d-on}(V_d, i, T_j) \tag{5.14}$$

$$V_{d-st} = f_{d-st}(i, T_j) \tag{5.15}$$

where
P_{s-on} = Power Losses during on time of the IGBT
P_{s-off} = Power Losses during off time of the IGBT
P_{d-on} = Power Losses during on state of the Diode
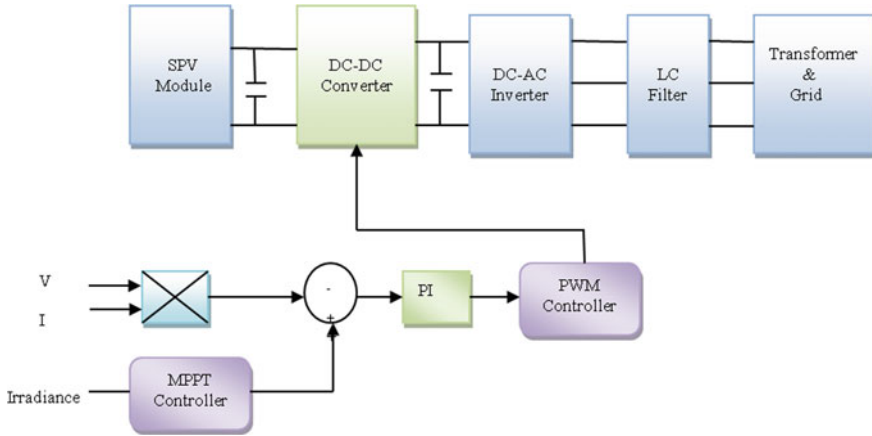P_{d-off} = reverses recovery losses of the Diode.

Fig. 5.15 PI controller based INC MPPT

5.7 Thermal Model

A state-space block is used to build a one-cell Cauer network modeling the thermal capacitance of the device junction as well as its junction-to-case thermal resistance. The state space equations are given below:

$$x' = \left[\frac{-1}{R_{th}C_{th}}\right]x + \left[\frac{1}{R_{th}C_{th}} \quad \frac{1}{C_{th}}\right]\begin{bmatrix}T_c \\ P_l\end{bmatrix} \tag{5.16}$$

$$\begin{bmatrix}T_j \\ P_c\end{bmatrix} = \begin{bmatrix}1 \\ \frac{1}{R_{th}}\end{bmatrix}x + \begin{bmatrix}0 & 0 \\ -\frac{1}{R_{th}} & 0\end{bmatrix}\begin{bmatrix}T_c \\ P_l\end{bmatrix} \tag{5.17}$$

where, T_j is junction temp of IGBT, P_l is power loss across IGBT, T_c is case temperature of IGBT, R_{th} is junction to case thermal resistance. C_{th} is thermal capacitance of junction; P_c is heat flow from junction to case. Now by calculating the junction temperature we can calculate the power losses of the IGBT. The same analysis is extended for power losses and junction temperature calculation of anti-parallel diode.

5.8 ANFIS Based Controllers

Classical PI and PID controllers that are used in conventional control are mainly tuned using specific methods. The design of the PI controller based INC MPPT is as shown in Fig. 5.15. Several methods provide initial values of the controller parameters. The most commonly used methods are based on the Ziegler-Nichols approach. However, these methods can be time consuming and fixed controllers
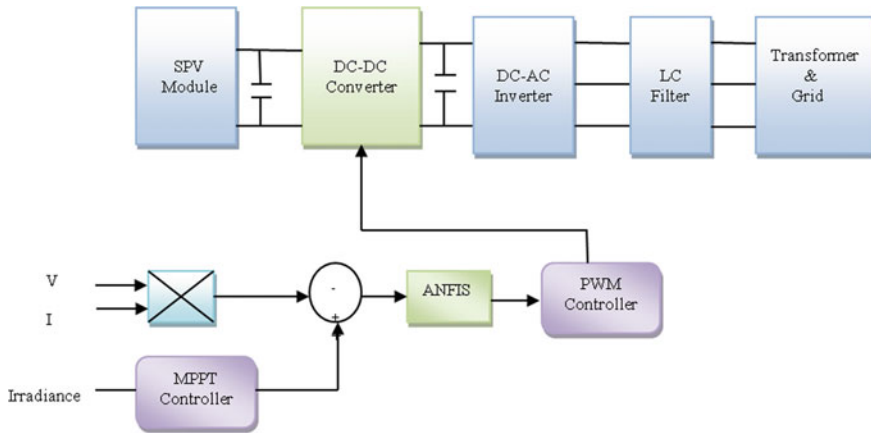
Fig. 5.16 ANFIS controller based INC MPPT

cannot necessarily provide acceptable dynamic performance over the complete operating range of the SPV system. Performance will degrade mainly because of factors such as system non-linearities and parameter variations. Adaptive controllers can be used to overcome these problems. Alternatively, performance-index based optimal control techniques can be adopted, but these may suffer from convergence related problems.

The purpose of using a computational intelligence based controller is to reduce the tuning efforts for improved response and to remove the shortcomings of conventional controllers. The design of the ANFIS controller is shown in Fig. 5.16. There are various possibilities to obtain the training data from the classical PI controlled transient simulation of the SPV system. The ANFIS controller is trained with the input and output data obtained from the transient simulations of the conventional PI controller with a wide range of operating conditions. The ANFIS controller acts like the conventional PI controller without the need to design and tune for different operating conditions repeatedly. The fuzzy logic toolbox in MATLAB^{TM} has been used for designing and testing the ANFIS controllers [41].

The Adaptive-Neuro Fuzzy Inference system is a hybrid system that combines the potential benefits of both the methods ANN and FL. This technique has been employed in numerous modeling and forecasting problems. ANFIS starts its functionality with the fuzzyfication of input parameters defining the membership function and design of fuzzy IF-THEN rules, by employing the learning capability of ANN for automatic fuzzy rules generation and self adjustment of membership functions [44].

In this work, the Sugeno method or Takagi-Kang method of fuzzy inference has been used. The Sugeno method was introduced in 1985 [45]. It is similar to the Mamdani method in many aspects. The first two parts of the fuzzy inference process, fuzzifying the inputs and applying the fuzzy operator are exactly the

Fig. 5.17 First order Sugeno-type inference system
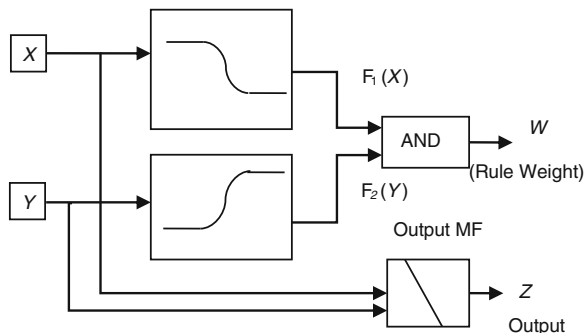
same. The difference is that unlike the mamdani method, in the sugeno method the output MFs are only constant or have linear relationship to the inputs. With a constant output MF, this method is known as the Zero-order Sugeno method, whereas with a linear relation, it is known as the first-order Sugeno method.

A typical rule in a Sugeno fuzzy model has the following form:

If Input-1 = x, and Input-2 = y, then, Output z = ax + by + c.

For a Zero-order Sugeno model, the output level z is a constant (a = b = 0). The output level zi of each rule is weighted by the firing strength w_i of the rule. For example, for an AND rule with Input-1 = x, and Input-2 = y, the firing strength is

w_i = AND (F1(x), F2(y)),

where F1 (.) and F2 (.) are the inputs for 1 and 2.

The final output of the system is the weighted average of the output of all the rules, computed as

$$\text{Final output} = \frac{\sum_{i=1}^{N} w_i z_i}{\sum_{i=1}^{N} w_i} = \sum_{i=1}^{N} g_i z_i, g_i = \frac{w_i}{\sum_{i=1}^{N} w_i} \tag{5.18}$$

A sugeno rule operates as shown in Fig. 5.17.

The basic structure of fuzzy inference system seen, so far, is a model that maps input characteristics to input membership functions, input membership function to rules, rules to a set of output characteristics, output characteristics to output membership functions, and the output membership function to a single-valued output or a decision associated with the output. In both Mamdani and Sugeno type of inference systems, when used for data modeling, membership functions and rule structure are essentially predetermined by the human interpretation of the characteristics of the variables of the data model.

The shape of the membership functions depends on the values of the parameters. Instead of just looking at the data to choose the membership function parameters, by using ANFIS membership function, the parameters can be chosen automatically. The basic idea behind neuro-adaptive learning techniques is very simple. These techniques provide a method for the fuzzy modeling procedure to learn information about a data set, in order to compute the membership function parameters that best allow the associated fuzzy inference system to track the given

Fig. 5.18 Typical ANFIS structure
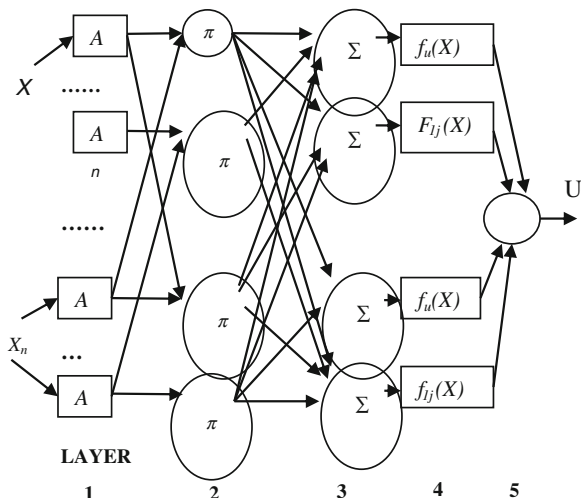
input/output data. This learning method works similar to the neural networks. In an adaptive neuro-fuzzy inference technique, using a given input/output data set, a fuzzy inference system (FIS) is constructed, whose membership function parameters are tuned (adjusted) using either a back-propagation algorithm alone, or in combination with a least squares type of method. This allows fuzzy systems to learn from the data. A network-type structure, similar to that of a neural network, which maps inputs through input membership functions and associated parameters, and then through output membership functions and associated parameters to outputs, can be used to interpret the input/output map.

Figure 5.18 shows the basic structure of the ANFIS algorithm for a first order Sugeno-type fuzzy system. The various layers shown in Fig. 5.18 are explained below [46].

Layer 1

Every node i, in this layer, is a square node with a node function

$$O_i^1 = \mu_{A_i}(x)$$

where, x is the input to node i, and A_i is the linguistic label (small, large, etc.,) associated with this node function. In other words, O_i^1 is the membership function of A_i and it specifies the degree to which the given x satisfies the quantifier A_i. Usually $\mu_{Ai}(x)$ is selected to be bell shaped with maximum value equal to 1, and minimum value equal to 0, such as

$$\mu_{A_i}(x) = \exp\left\{ -\left(\frac{x - c_i}{a_i} \right)^2 \right\}$$

where, $\{a_i, b_i, c_i\}$ is the parameter set. As the values of these parameters change, the bell-shaped functions vary accordingly, thus exhibiting various forms of

membership functions on linguistic label A_i. In fact any piecewise differentiable function, such as commonly used trapezoidal or triangular-shaped membership function, is also qualified candidates for node functions in this layer. Parameters in this layer are referred to as premise parameters.

Layer 2

Every node in this layer is a circle node, labeled $\prod$, which multiplies the incoming signals and sends the product out. For example $w_i = \mu_{A_i}(x) X \mu_{B_i}(y)$, $i = 1, 2$. Each node output represents the firing strength of a rule. In fact, other T-norm operators that performs generalized AND can be used as the node function in this layer.

Layer 3

Every node in this layer is a circle node, labeled N. The *i*th node calculates the ratio of the *i*th rule's firing strength to the sum of all rule's firing strengths, as given below.

$\overline{w_i} = \frac{w_i}{w_1 + w_2}, i = 1, 2$ Outputs of this layer are known as normalized firing strengths.

Layer 4

Every node i in this layer is a square node with a node function

$$O_i^4 = w_i f_i = w_i(p_i x + q_i y + r_i)$$

where, $\overline{w_i}$ is the output of layer 3, and $\{p_i, q_i, r_i\}$ is the parameter set. Parameters in this layer will be referred to as consequent parameters.

Layer 5

The single node in this layer is a circle node labeled Σ that computes overall output as the summation of all incoming signals, i.e.

$$O_i^5 = {}_i \ overall \ output = \sum_i \overline{w_i} f = \frac{\sum_i w_i f_i}{\sum_i w_i} \tag{5.19}$$

The adjustment of modifiable parameters is a two-step process. First, information are propagated forward in the network until Layer-4, where the parameters are identified by a least-squares estimator. Then, the parameters in Layer-2 are modified using gradient descent. The only user specified information is the number of membership functions in the universe of discourse for each input and output as training information. ANFIS uses back propagation learning to learn the parameters related to membership functions and least mean square estimation to determine the consequent parameters. Every step in the learning procedure includes two parts. The input patterns are propagated, and the optimal consequent parameters are estimated by an iterative least mean square procedure. The premise parameters are assumed fixed for the current cycle through the training set. The pattern is propagated again, and in this epoch (iterations), back propagation is used to modify the premise parameters, while the consequent parameters remain fixed.

The parameters associated with the membership functions will change through the learning process. The computation of these parameters (or their adjustment) is facilitated by a gradient vector, which provides a measure of how well the fuzzy

Table 5.3 System parameters

| T_{PV}	Temperature of PV cells	25 °C
G	Irradiance of PV cells	1 kW/m^2
C_{PV}	Boost capacitance	100 μF
C_{DC}	DC link capacitance	6 mF
L_{LC}	Inductance of the LC filter + resistance	250 μH + 2 mΩ
F_{req}	Inverter switching frequency	1.65 kHz
V_{grid}	Grid RMS voltage	25 kV
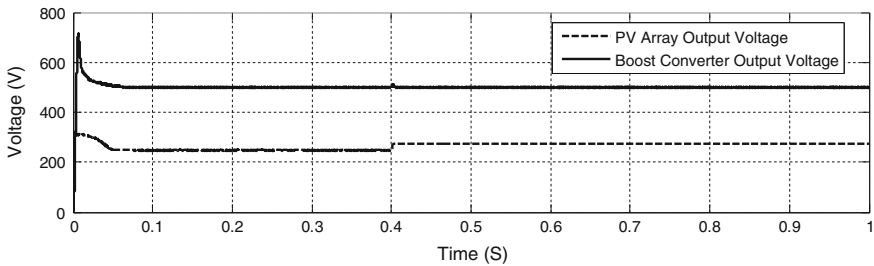
Fig. 5.19 DC output voltage of PV array DC–DC boost converter

inference system is modeling the input/output data for a given set of parameters. Once the gradient vector is obtained, some of the available optimization routines can be applied to adjust the parameters so as to reduce some error measure (usually defined by the sum of the squared difference between actual and desired outputs).

The big advantage of the Sugeno-type FIS, is that it avoids the use of time consuming defuzzification, since it is a more compact and computationally efficient representation than the Mamdani system, the Sugeno system lend itself to the use of adaptive technique for construction fuzzy models. Theses adaptive technique can be used to customize the MFs so that fuzzy system accurately models the data. Some of the advantages of the Sugeno-type method are that it is computationally efficient; it works well with linear techniques (e.g., PID control).

5.9 Performance Comparisons

The schematic diagram of the main system of 100.7 kW is shown in Fig. 5.1. The modeling and simulation has been done using Matlab/Simulink software. The main system parameters are given in Table 5.3. The system is simulated with zero initial conditions hence results are settling down to steady-state values after transient period. The MPPT algorithms have been activated at the 0.4 s instant. The SPV array has been simulated and the steady state voltage output is 240 V and the boost converter has been used to boost the voltage level at steady-state without MPPT as shown in Fig. 5.19. The operating voltage of the SPV array increases after using
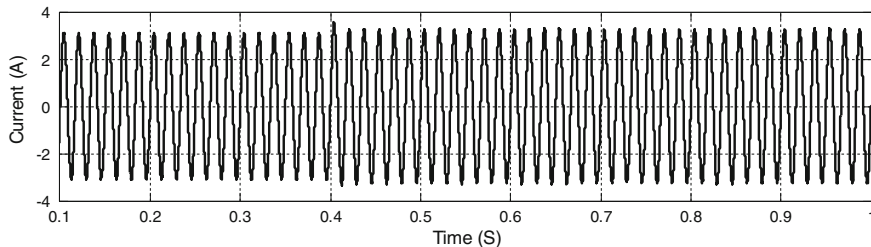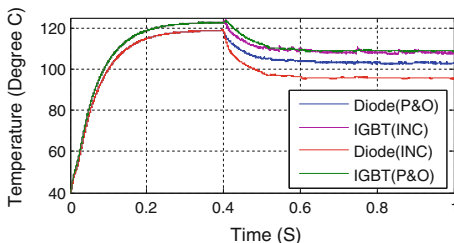
Fig. 5.20 Grid injected current

**Fig. 5.21** Comparison of energy injected into the grid
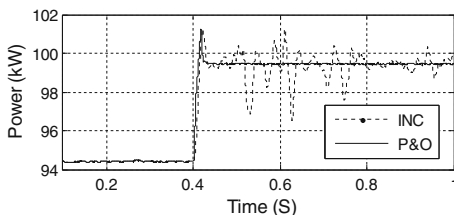
**Fig. 5.22** Comparison of junction temperature of IGBT and diode

MPPT algorithms (MPPT algorithm starts at 0.4 s). The grid current follows the sinusoidal waveform as shown in Fig. 5.20 and the Total Harmonic Distortion (THD) is 1.66 % which is acceptable as per the IEEE-519 standard.

The energy injected into the grid using INC method is better than P&O method and the efficiency of the SPV system is 99.11 % using INC MPPT as compared to P&O MPPT having efficiency of 99.06 %. The Fig. 5.21 clearly show the advantage of using MPPT algorithms, as energy injected into the grid has increased from 95.6 kW to almost 100.7 kW after the instant 0.4 s when MPPT algorithms activated. The Fig. 5.22 shows the comparison of junction temperature of IGBT and DIODE using INC and P&O MPPT. It clearly indicates that without MPPT the junction temperature is high and the junction temperature of IGBT and DIODE are less using INC MPPT as compared to P&O MPPT. The switching losses of the DC–DC boost converter are higher in absence of MPPT algorithms as shown in Fig. 5.23 initially during transient state the switching losses are increasing exponentially and after some time they become constant. When the
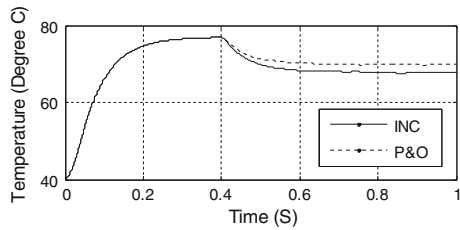
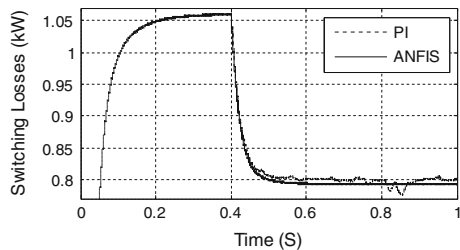**Fig. 5.23** Comparison of switching losses of IGBT and diode
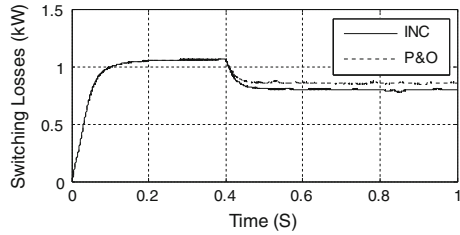
Fig. 5.24 Comparison of case temperature of IGBT and diode
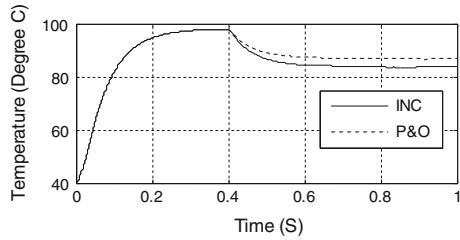
Fig. 5.25 Comparison of sink temperature of IGBT and diode


Fig. 5.26 Comparison of switching losses using PI and ANFIS controller

MPPT is on (at 0.4 s as shown in Fig. 5.23) the switching losses starts decreasing. The switching losses are less using INC MPPT as compared to P&O MPPT.

The Figs. 5.24 and 5.25 clearly indicates that the case and sink temperature of switching devices are also less using INC MPPT as compared to P&O MPPT in the DC–DC converter. The switching losses of the IGBT module in DC–DC boost converter start decreasing after the application of MPPT algorithm (at 0.4 s) as shown in the Fig. 5.26. The Fig. 5.26 clearly indicates that the switching losses using ANFIS controller in INC Algorithm are less as compared to the PI controller.

Fig. 5.27 Comparison of junction temperature of IGBT and diode using PI and ANFIS controller
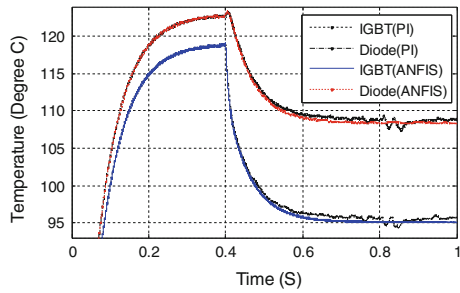
Fig. 5.28 Comparison of case temperature for PI and ANFIS controller
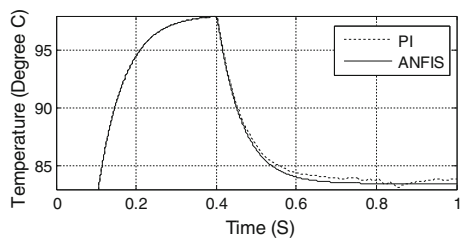
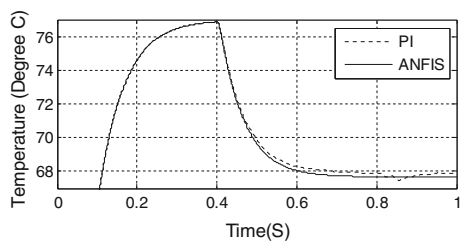**Fig. 5.29** Comparison of sink temperature of PI and ANFIS controller

The junction temperature of the IGBT module (Including IGBT and FD) is very important. Figure 5.27 clearly indicates that the junction temperature if IGBT module start decreasing when MPPT is activated. The junction temperature of IGBT module is less using ANFIS controller as compared to PI controller. The case temperature is also less using ANFIS controller as compared to PI controller as shown in the Fig. 5.28. As the Fig. 5.29 clearly indicates that the sink temperature is also less using ANFIS controller as compared to PI controller.

5.10 Concluding Remarks

This chapter presents a performance analysis of grid connected SPV system for different MPPT algorithms. The SPV array output injected into grid can be maximized using MPPT control systems, which consist of a power conditioner to

interface the PV output to grid and a control unit which derives the power conditioner such that it extracts the maximum power from a PV array. In this chapter, two different Maximum Power Point Tracking (MPPT) algorithm, Incremental Conductance (INC) and Perturb and Observe (P&O) MPPT algorithm are compared for DC–DC boost converter. Present work first gives the detailed mathematical model of grid connected three-phase SPV system. A parametric model of SPV cell is also presented. Second, thermal modeling and switching loss calculation of switching devices has been discussed and then the performance evaluations are be carried out for P&O and INC based MPPT algorithms for various operating conditions of the SPV array, in terms of energy injected to grid, switching losses, junction temperature and sink temperature, for switching in the DC–DC boost converter. Using the method of loss calculation, the power loss of IGBT and junction temperature can be estimated in the power conversion system. It can be used to improve the efficiency of the system and the ultimate thermal design. Also it can predict the working temperature of the IGBT and diode devices in order to avoid faults of the devices. The simulation result shows that the MPPT algorithms increase the SPV output energy injected into the grid. The switching losses and junction temperature of the switches are calculated and compared with two different MPPT algorithms. The performance of INC found to be better as compared to P&O. Later, in this present work, a nonlinear adaptive neuro-fuzzy inference system (ANFIS) is proposed to control the DC–DC boost converter instead of a conventional PI controller. The ANFIS have been trained with the input and output data of the conventional PI controller for different operating conditions. The training of ANFIS controllers has been done by combining the back-propagation gradient descent learning algorithm to choose the parameters related to membership functions and the least-squares estimation to determine the consequent parameters. Performance of the system is compared with two different controllers, i.e. (PI and ANFIS). The simulation result shows that the performance of the system in terms of switching losses, junction temperature, sink temperature and case temperature are better using ANFIS controller as compared to PI controller.

The vast potential of Computational Intelligence (CI) based techniques has yet to be explored for power electronic systems control applications. Hybrid CI techniques, particularly neuro-fuzzy techniques, have enormous potential for application. Similarly, there are numerous MPPT techniques are available in literature and practice, associated with many respective advantages and disadvantages. The area is vast, and the authors provided a discussion on the subjects which are the most relevant to the SPV system.

References

1. Esram T, Chapman PL (2007) Comparison of photovoltaic array maximum power point tracking techniques. IEEE Trans Energy Convers Summer Meet 22(2):439–449
2. Liu F, Duan S, Liu F, Liu B, Kang Y (2010) A variable step size INC MPPT for PV system. IEEE Trans Ind Electron 55:2622–2628
3. Data Sheet, IGBT Module U-Series 1200/600A, 1MBI600UB-120
4. Dell'Aquila RV, Balboni L (2010) A new approach: modelling simulation, development and implementation of a commercial grid-connected transformerless PV inverter. In: International symposium on power electronics, pp 1422–1429
5. Schoeman JJ, vanWyk JD (1982) A simplified maximal power controller for terrestrial photovoltaic panel arrays. In: 13th Annual IEEE power electronics specialists conference, pp 361–367
6. Buresch M (1983) Photovoltaic energy systems. McGraw Hill, New York
7. Hart GW, Branz HM, Cox CH (1984) Experimental tests of open loop maximum-power-point tracking techniques. Solar Cells 13:185–195
8. Patterson DJ (1990) Electrical system design for a solar powered vehicle. In: Proceedings of 21st annual IEEE power electronics conference, pp 618–622
9. Masoum MAS, Dehbonei H, Fuchs EF (2002) Theoretical and experimental analysis of photovoltaic systems with voltage and current based maximum power point tracking. IEEE Trans Energy Convers 17(4):514–522
10. Noh H-J, Lee D-Y, Hyun D-S (2002) An improved MPPT converter with current compensation method for small scaled PV-applications. In: Annual conference on industrial electronic society, pp 1113–1118
11. Kobayashi K, Matsuo H, Sekine Y (2004) A novel optimum operating point tracker of the solar cell power supply system. In: IEEE power electronics specialists conference, pp 2147–2151
12. Bekker B, Beukes HJ (2004) Finding an optimal PV panel maximum power point tracking method. In: 7th AFRICON conference in Africa, pp 1125–1129
13. Noguchi T, Togashi S, Nakamoto R (2000) Short-current pulse based adaptive maximum-power-point tracking for photovoltaic power generation system. In: IEEE international symposium on industrial electronics, pp 157–162
14. Mutoh N, Matuo T, Okada K, Sakai M (2002) Prediction-data-based maxi mum-power-point-tracking method for photovoltaic power generation systems. In: IEEE power electronics specialists conference, pp 1489–1494
15. Yuvarajan S, Xu S (2003) Photo-voltaic power converter with a simple maximum-power-point-tracker. In: International symposium on circuits and system, pp 399–402
16. Wasynczuk O (1983) Dynamic behaviour of a class of photovoltaic power systems. IEEE Trans Power App Syst 102(9):3031–3037
17. Hua C, Lin JR (1996) DSP-based controller application in battery storage of photovoltaic system. In: IEEE IECON 22nd international conference on industrial electronics, pp 1705–1710
18. Slonim MA, Rahovich LM (1996) Maximum power point regulator for 4 kW solar cell array connected through inverter to the AC grid. In: 31st intersociety energy conversion eng conf, pp 1669–1672
19. Al-Amoudi A, Zhang L (1998) Optimal control of a grid-connected PV system for maximum power point tracking and unity power factor. In: 7th international conference on power electronics and variable speed drives, pp 80–85
20. Kasa N, Iida T, Iwamoto H (2000) Maximum power point tracking with capacitor identifier for photovoltaic power system. In: 8th international conference on power electronics and variable speed drives, pp 130–135

21. Zhang L, Al-Amoudi A, Bai Y (2000) Real-time maximum power point tracking for grid-connected photovoltaic systems. In: 8th international conference on power electronics variable speed drives, pp 124–129
22. Hua C-C, Lin J-R (2001) Fully digital control of distributed photovoltaic power systems. In: IEEE international symposium on industrial electronics, pp 1–6
23. Chiang M-L, Hua C-C, Lin J-R (2002) Direct power control for distributed PV power system. In: Proceedings of power conversion conference, pp 311–315
24. Chomsuwan K, Prisuwanna P, Monyakul V (2002) Photovoltaic grid connected inverter using two-switch buck-boost converter. In: 29th IEEE photovoltaic specialist conference, pp 1527–1530
25. Hsiao Y-T, Chen C-H (2002) Maximum power tracking for photovoltaic power system. In: 37th IAS annual meeting of industry application conference, pp 1035–1040
26. Boehringer AF (1968) Self-adapting dc converter for solar spacecraft power supply. IEEE Trans Aerosp Electron Syst 4(1):102–111
27. Costogue EN, Lindena S (1976) Comparison of candidate solar array maximum power utilization approaches. In: Intersociety energy conversion engineering conference, pp 1449–1456
28. Harada J, Zhao G (1989) Controlled power-interface between solar cells and ac sources. In: IEEE telecommunication power conference, pp 22.1/1–22.1/7
29. Hussein KH, Mota I (1995) Maximum photovoltaic power tracking: An algorithm for rapidly changing atmospheric conditions. In: IEE proceedings on generation, transmission and distribution, pp 59–64
30. Brambilla A, Gambarara M, Garutti A, Ronchi F (1999) New approach to photovoltaic arrays maximum power point tracking. In: 30th annual IEEE power electronics specialist conference, pp 632–637
31. Irisawa K, Saito T, Takano I, Sawada Y (2000) Maximum power point tracking control of photovoltaic generation system under non-uniform isolation by means of monitoring cells. In: 28th IEEE photovoltaic specialist conference, pp 1707–1710
32. Kim T-Y, Ahn H-G, Park SK, Lee Y-K (2001) A novel maximum power point tracking control for photovoltaic power system under rapidly changing solar radiation. In: IEEE international symposium on industrial electronics, pp 1011–1014
33. Kuo Y-C, Liang T-J, Chen J-F (2001) Novel maximum-power-point tracking controller for photovoltaic energy conversion system. IEEE Trans Ind Electron 48(3):594–601
34. Yu GJ, Jung YS, Choi JY, Choy I, Song JH, Kim GS (2002) A novel two-mode MPPT control algorithm based on comparative study of existing algorithms. In: 29th IEEE photovoltaic specialist conference, pp 1531–1534
35. Kobayashi K, Takano I, Sawada Y (2003) A study on a two stage maximum power point tracking control of a photovoltaic system under partially shaded insolation conditions. In: IEEE power engineering society general meeting, pp 2612–2617
36. Wilamowski BM, Li X (2002) Fuzzy system based maximum power point tracking for PV system. In: 28th annual conference on IEEE industrial electronics, pp 3280–3284
37. Veerachary M, Senjyu T, Uezato K (2003) Neural-network-based maximum-power-point tracking of coupled-inductor interleaved-boost converter-supplied PV system using fuzzy controller. IEEE Trans Ind Electron 50(4):749–758
38. Khaehintung N, Pramotung K, Tuvirat B, Sirisuk P (2004) RISC microcontroller built-in fuzzy logic controller of maximum power point tracking for solar-powered light-flasher applications. In: 30th annual conference on IEEE industrial electronics society, pp 2673–2678
39. Ro K, Rahman S (1998) Two-loop controller for maximizing performance of a grid-connected photovoltaic-fuel cell hybrid power plant. IEEE Trans Energy Convers 13(3):276–281
40. Hussein A, Hirasawa K, Hu J, Murata J (2002) The dynamic performance of photovoltaic supplied dc motor fed from DC–DC converter and controlled by neural networks. In: International joint conference on neural network, pp 607–612

41. Sun X, Wu W, Li X, Zhao Q (2002) A research on photovoltaic energy controlling system with maximum power point tracking. In: Power conversion conference, pp 822–826
42. Zhang L, Bai Y, Al-Amoudi A (2002) GA-RBF neural network based maximum power point tracking for grid-connected photovoltaic system. In: International conference on power electronics machines and drives, pp 18–23
43. Xu D, Lu H, Hung Liu L, Azuma SS(2010). Power losses and junction temperature analysis of power semiconductor devices. IEEE Trans Ind Electron 38(5):1426–1431
44. Afgoul H, Krim F (2012) Intelligent energy management in a photovoltaic installation using neuro-fuzzy technique. In: IEEE ENERGYCON conference and exhibition, pp 20–25
45. Sugeno M (1993) Industrial applications of fuzzy control. Elsevier Science Publication, Amsterdam
46. Shing J, Jang R (1993) ANFIS: adaptive-network based fuzzy inference system. IEEE Trans Syst Man 23:665–685